Paper 19-2 has been designated as a Distinguished Paper at Display Week 2025. The full-length version of this paper appears in a Special Section of the *Journal of the Society for Information Display (JSID)* devoted to Display Week 2025 Distinguished Papers. This Special Section will be freely accessible until December 31, 2025 via:

https://sid.onlinelibrary.wiley.com/doi/full/10.1002/jsid.2083

Authors that wish to refer to this work are advised to cite the full-length version by referring to its DOI:

https://doi.org/10.1002/jsid.2083

All Inkjet-Printed QD-LED Display with High-Resolution of 264 ppi

Dong Jin Kang, Dong-Ha Lee, Seunghwa Jeong, Eun-A Yang, Jongjang Park, Kyeongseo Min, Giho Kang, Jaekwon Hwang, Yul-Guk Kim, Jaehyun Park, Donghoon Kwak, Sehun Kim, Hyunchul Kang, Tanaka Masanobu, Yeo-geon Yoon, and Changhee Lee**

Display Research Center, Samsung Display Co., Ltd., Giheung-gu, Yongin-City, Gyeonggi-Do, Korea

Abstract

Inkjet printing enables high-precision patterning for QD-LED displays, but there are many technological challenges for achieving high pixel densities. We developed advanced inkjet printing processes for fabricating high-resolution 264-ppi QD-LED displays. This work paves the way for large-scale production of high-quality QD-LED displays suitable for premium IT products, including tablets and laptops.

Author Keywords

Quantum dot light-emitting diodes; ink-jet printing, high-resolution; jetting properties; top emission;

1. Introduction

Inkjet printing technology offers remarkable versatility in handling diverse ink materials and enables the direct creation of intricate, customized patterns on substrates without requiring masks or other patterning techniques. Its scalability for high-volume production aligns well with the increasing demand for premium display products. This adaptability makes inkjet printing a valuable technique in various stages of quantum dot (QD) display fabrication, from patterning QD color conversion layers (CCL) to producing entire QD light-emitting diode (QD-LED) structures [1-3]. However, current resolution limitations of inkjet printing method constrain its application to products that require high-resolution displays, such as tablets and smartphones. Substantial technological advancement in overcoming this hurdle is necessary to position inkjet printing as a competitive alternative to vacuum deposition techniques [4].

Achieving a high-resolution inkjet-printing requires precise drop placement, consistent ejected droplet volume, and a controlled ink drying speed. Given the interdependence of these factors, it is essential to develop printing and drying processes that address their combined effects. A significant challenge involves an ink formulation enabling multi-layer QD-LED structures. Inks containing charge-transporting materials and QDs must possess optimal physicochemical properties for stable jetting and drying, ensuring droplet formation, wettability, and reproducibility [4]. Moreover, the demanding nature of printing and drying processes, involving exposure to various solvents and heat, can degrade materials, adversely affecting display performance. It is critical to ensure robust layer deposition without compromising QD integrity or charge-transporting functionality due to solvent interactions. Addressing these challenges requires the careful design of ligands, additives, and solvents that optimize device performance while safeguarding material stability and functionality.

Here, we demonstrate the development of all inkjet-printed 6.55-inch full-color QD-LED displays with 264 ppi, the highest resolution achieved to date using inkjet printing processes [5-7], as shown in Figure 1. Ink properties are optimized for inkjet printing processes and a printing algorithm is tailored for high-resolution patterning. And post-printing processes, such as drying and thermal baking, are controlled to obtain improved device performance.

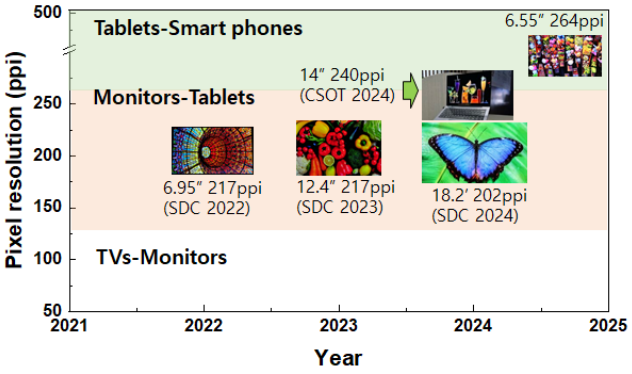

Figure 1. Recent development of high-resolution QD-LED (EL-QD) displays reported in the SID symposiums.

2. Results and Discussion

The physical properties of inks for high-resolution inkjet processes can be characterized through the dimensionless *Z* number in fluid mechanics. The fluid is stable to make a drop for $1 < Z < 10$ [8]. To ensure successful ink jetting, surface tension and viscoelastic characteristics were optimized, taking into account the printing head surface. Table 1 shows the basic ink properties of hole injection layer (HIL), hole transport layer (HTL), light-emitting layer (QDs), and inorganic complex electron transport layer (ETL). A linear dispensing volume was observed in response to the applied voltage, allowing for control of the film thickness by adjusting the dispensing volume at different voltages. Since each ink exhibited different rheological properties, specific waveform tuning was conducted for each ink. This allowed for the precise control of ink volume during the printing process. The ink drying and thermal baking conditions such as chamber temperature and pressure were controlled to obtain targeted film thickness with the in-pixel uniformity.

Table 1. Rheological properties of inks at 25℃

Rheological properties	HIL	HTL	QDs	ETL
Surface tension (mN/m)	30.9	25.6	30.8	28.3
Viscosity (mPa·s)	2.64	4.9	6.80	10.3
Density (g/cm^3)	0.90	0.97	0.94	0.94
Nozzle diameter (μm)	12	12	12	12
Z number	8.82	3.52	3.50	1.74

ISSN 0097-996X/25/5601-0232-$1.00 © 2025

The ink properties and dispensing consistency within the head was evaluated using a piezo axial vibrator (PAV). The PAV is a powerful tool to obtain the fluid properties (modulus, and viscosities) at the high frequencies although oscillatory rheometer can get the fluid properties at relatively low frequencies. Moreover, since the PAV has the same piezoelectric method as the piezoelectric inkjet printer, it has a great advantage in characterizing the fluid properties of a sample. The complex squeeze stiffness K^* of the sample is calculated by the dynamic displacement with and without the loading samples with constant force amplitude [9].

$$K^* = \frac{3\pi}{2} R \left(\frac{R}{d}\right)^3 G^* / \left(1 + \frac{\rho\omega^2 d^2}{10G^*} + \cdots\right) \quad (1)$$

where R is the radius of the plate, d is the gap between the top plate and bottom plate, p is the density of the sample, and G^* is complex modulus of the sample with $G^*=G'+iG''$, whre G' is the storage modulus and G'' is the loss modulus.

The complex viscosities, η^*, of QD and HIL inks are plotted in Fig. 2. The η^* of QD is higher than that of HIL within the measurable frequency range (from 100 Hz to 3 kHz) of PAV. The η^* of QD is 6.80 mPa·s at 25℃ and 500 Hz, higher than that of HIL (2.64 mPa·s). As viscosities between QD and HIL are different, the optimized jetting conditions are different.

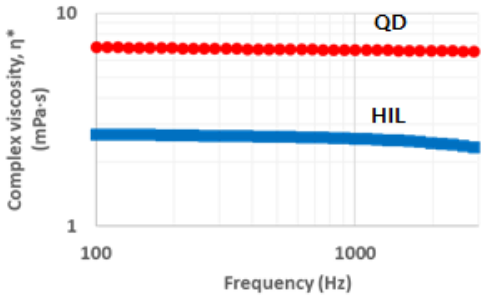

Figure 2. The η* of the QD, HIL samples

The analysis of unique waveform of sample is useful when designing inkjet printing conditions [10]. The waveforms of QD and HIL inks are shown in Figure 3. The higher peak amplitude value of the HIL ink compared to the QD ink (297.9 mV and 280.2 mV for QD and HIL, respectively, in Table 2) implies that HIL gets more energy than QD at the same input drive voltage. Thus, QD needs higher driving voltage than HIL to achieve the same drop velocity. In addition, the relaxation time of the inks are 28.34μs for QD and 39.85μs for HIL, respectively. The total times from the start to the end time of waveforms were calculated by adding peak time and relaxation time. The realistic print frequencies, reciprocal of the total time, of the inks were obtained to be 29.68 kHz and 22.13 kHz for QD and HIL, respectively. Compared to traditional organic inks, distinct behaviors were observed in QD inks, particularly in terms of solvent interactions and particle-induced agglomeration due to rheological properties. The oscillation before and after dispensing was found to be rapidly stabilized with varying voltage application time. The rapid stabilization directly correlates with productivity improvement in mass production.

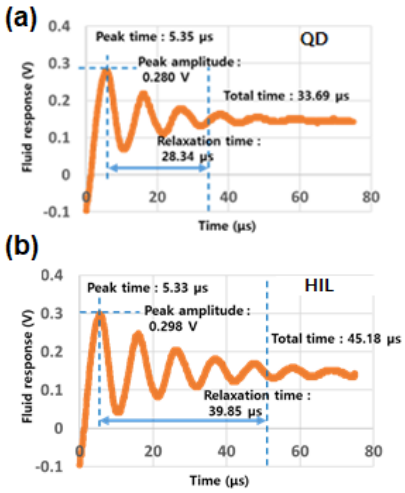

Figure 3. Waveforms of (a) QD and (b) HIL at 25℃

Table 2. Waveform features of QD and HIL at 25℃

	QD	HIL
Peak time (μs)	5.35	5.30
Peak amplitude (mV)	280.2	297.9
Relaxation time (μs)	28.34	39.85
Dwell time (μs)	4.0	4.0
Driving voltage (V)	30	20

Figure 4 describes the printing algorithm to produce a 264 ppi panel. The ink droplet must be landed within the pixel-definable layer (PDL). Based on our R/G/B pixel arrangement, necessary landing accuracy was calculated to be within 18μm. Because the pixel size of our panel is relatively small, actual landing accuracy was adjusted within 9.59 μm as shown in Figure 4 (a). There was a deviation according to the ejected volume variation and repetition due to the difference in physical characteristics between organic and inorganic inks, as shown in Figure 4(b). The volume deviation of the organic material ink was greater than that of the particle dispersed ink (5.3% for HIL vs 1.9% for QD ink), owing to the change in rheological properties of polymer-type HTL ink induced by the shear force.

To achieve high resolution printing, we employed the drive per nozzle (DPN) function and nozzle mixing technique as shown in Figure 4(c) and (d) [11]. DPN allows for the generation of the desired range of drop volumes by iteratively measuring the volume of drops ejected from individual nozzle and adjusting the waveform accordingly. For instance, Yoshida et al. reported that their DPN printheads obtained a pixel volume variation of < ± 0.8% under mass production conditions with organic inks [12]. Nozzle mixing of about 400 nozzles resulted in randomly deposited ink droplets in a specific order. The jetting deviation of each nozzle was evaluated to ensure uniform thickness formation within pixels. Adjusting the 2 pL nozzle arrangement minimized thickness variation between adjacent pixels. As a result, the total volume of HIL, HTL, QD, ETL inks is effectively controlled to reduce printing mura as shown in Figure 4(e). And the drop volume variation of all inks can be achieved as low as ± 2.5%.

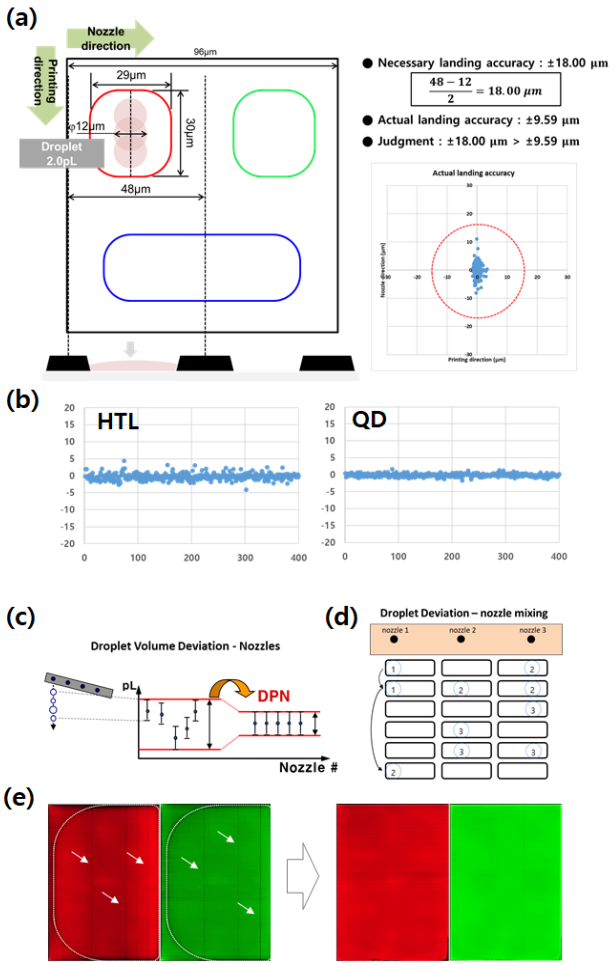

Figure 4. (a) 6.55" 264 ppi pixel structure and high resolution printing algorithm, (b) pixel volume variation of HTL and QD. (c) schematic illustration of DPN technique, (e) schematic illustration of nozzle mixing method, (e) before and after applying DPN and nozzle mixing techniques,

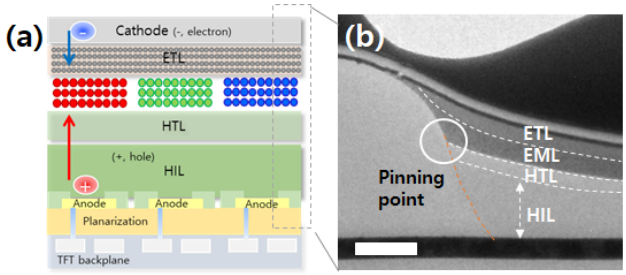

Figure 5. (a) Device structure of 6.55" 264ppi RGB QD-LED display, (b) FIB-SEM cross-section pixel image and pinning point. The scale is 500 nm.

The inkjet device structure used in this study is a top-emitting device, optimized by varying the thicknesses of R/G/B subpixels. As illustrated in Figure 5(a), the differential thickness adjustment across the entire device structure was achieved through the HIL layer. Surface energy differences within the pixels confine the ink, with pinning occurring at the pixel edges. Differences in the pinning points and fluid dynamics due to the different ink volume within the pixel PDLs resulted in distinct film profiles as shown in Figure 5(b). We found that the profile of QD film is closely related to the device characteristics, particularly its luminous area, which greatly influences both efficiency and lifetime.

To maximize the emission area, the morphology of inkjet-printed layer should be flat and smooth. Most of film morphologies shown in Figure 6(a), however, indicate U and W shapes after performing all drying processes under high-vacuum level (~1×10^{-6} torr) and a higher temperature (~45°C). Slow drying process at low pressure (under ~1×10^{-1} torr) may be helpful for the flattening of the film morphology, but the slow drying speed can produce drying mura due to the difference in drying speed between the edge and the center of the panel, as shown in Figure 6(b). Thus, maintaining a fast drying speed is necessary for removing the entire mura of the device. Completing all drying process in tens of seconds also improves the productivity of mass production. Thus, we employed a fast drying process even though unflattened film shape was formed. Further tuning of ink properties and drying conditions will be carried out for producing mura-free inkjet-printed QD-LED display panels with improved in-pixel uniformity. After drying process, thermal baking was conducted at 180°C in an oxygen-limited environment to prevent oxidation. Thermal baking facilitated solvent removal, molecular reorganization, and film densification, which reduced defects, and enhanced charge transport.

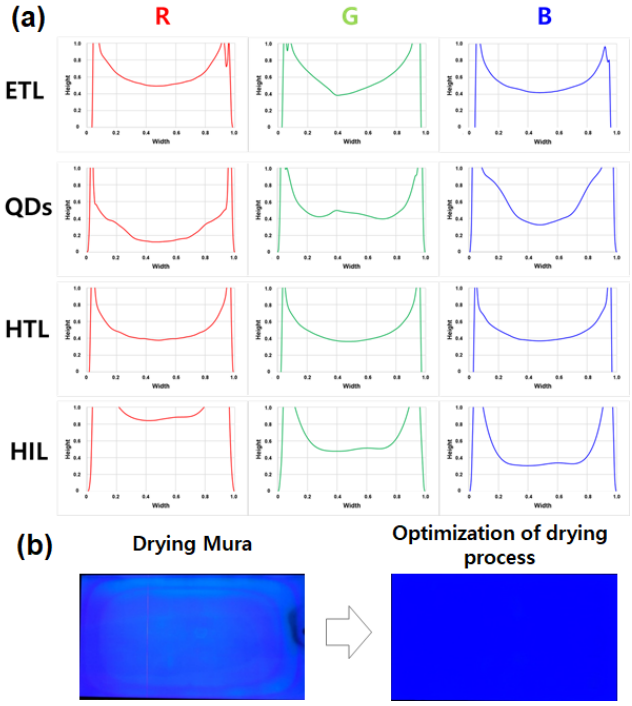

Figure 6. (a) Morphologies of each layer in the RGB pixels after vaccum drying process. (b) Optimization of drying process to remove drying mura.

Figure 7 shows 6.55-inch full color QD-LED display with 264ppi resolution using advanced inkjet printing technology. The characteristics of luminance efficiency is comparable to our previous work [6]. The external quantum efficiency (EQE) of R/G/B devices are 29.2, 82.0, and 9.3 cd/A, respectively.

Figure 7. Image of 6.55” full color EL-QD display panel with 264 ppi resolution.

3. Conclusion

We demonstrated 6.55" full-color QD-LED displays with 264 ppi, the highest resolution achieved to date with using all inkjet printing process. This work paves the way for producing high-quality QD-LED displays suitable for products that require high-resolution displays, such as tablets and smartphones. With advancements in QDs, ink formulations, device engineering, and inkjet-based mass production techniques, QD-LED displays are becoming increasingly cost-effective, facilitating broader market adoption. Although widespread adoption may take time, the transformative potential of QD-LEDs in the display industry is undeniable.

4. References

[1] Park, M., Kim, T. H., Jun, S., Lee, C. QD Light-Emitting Diodes: An Overview and Their Impact on the Display Landscape, *Inf. Display*, 2024; 40 (3): 32-37

[2] Kim, J., et. Al., Recent Advances and Challenges of Colloidal Quantum Dot Light-Emitting Diodes for Display Applications. *Adv. Mater.* 2023 2212220.

[3] Qian, L., *et al.*, 6-2: Invited Paper: Key Challenges towards the Commercialization of Quantum-Dot Light-Emitting Diodes. *SID Int. Symp. of Dig. Tech. Papers*. 2017; 48(1): 55—57.

[4] Han, C., et al., Inkjet-printed quantum dot light-emitting diodes: Development and challenges for display applications. *J. Soc. Inf. Display*. 2024; 32: https://doi.org/10.1002/jsid.2006.

[5] Park M, et al., All inkjet-printed 6.95″ 217 ppi active matrix QD-LED display with RGB Cd-free QDs in the top-emission device structure. *J. Soc. Inf. Display*. 2022; 30(5): 433–440.

[6] Ha J, et al., Dual ligand exchange of Cd-free quantum dots and optimal control of ink formulation for improving the performance of all-inkjet-printed quantum dot light-emitting diodes. *J. Soc. Inf. Display*. 2024; 32(5): 332–340.

[7] Chris Hauf., SID Award for Inkjet-Printed QD-EL Display, https://kateeva.com/sid-award-for-inkjet-printed-qd-el-display/, 2024.

[8] Kang DJ, et.al., Soft electronics by inkjet printing metal inks on porous substrates. *Flex. Print. Electron*. 2022; 7(3):03300

[9] Jérôme J. Crassous. Characterization of the viscoelastic behavior of complex fluids using the piezoelastic axial vibrator. *Journal of Rheology*, 2005 **49**, 851-863

[10] Aamir Hamad. Characteristics of nanosilver ink (UTDAg) microdroplets and lines on polyimide during inkjet printing at high stage velocity. *Materials Advances*, 2020, **1**, 99-107

[11] Kang, D. J. and Lee, C. Chapter 10. QD LED lanel process: Inkjet printing. 2025, Wiley, In press

[12] Yoshida H, et. al., Mura-free G8.5 220ppi inkjet printing technology for OLED and QLED display panels. *J. Soc. Inf. Display*. 2024; 32(5): 255–266.